Molecular scale study on the interactions of biocompatible nanoparticles with macrophage membrane and blood proteins

Khedri, Mohammad; Afsharchi, Fatemeh; Souderjani, Amirhosein Hasanpour; Rezvantalab, Sima; Didandeh, Mohsen; Maleki, Reza; Musaie, Kiyan; Santos, Hélder A.; Shahbazi, Mohammad-Ali

Published in:
Nano Select

DOI:
10.1002/nano.202200043

Publication date:
2022

Received: 24 February 2022 | Revised: 6 April 2022 | Accepted: 19 April 2022

DOI: 10.1002/nano.202200043

RESEARCH ARTICLE

Nano Select WILEY

Molecular scale study on the interactions of biocompatible nanoparticles with macrophage membrane and blood proteins

Mohammad Khedri[1] | **Fatemeh Afsharchi**[2] | **Amirhosein Hasanpour Souderjani**[3] | **Sima Rezvantalab**[4] | **Mohsen Didandeh**[5] | **Reza Maleki**[1] | **Kiyan Musaie**[2] | **Hélder A. Santos**[6,7,8] | **Mohammad-Ali Shahbazi**[6,7]

[1]Computational Biology and Chemistry Group (CBCG), Universal Scientific Education and Research Network (USERN), Tehran, Iran

[2]Zanjan Pharmaceutical Nanotechnology Research Center (ZPNRC), Zanjan University of Medical Sciences, Zanjan, Iran

[3]Department of Pharmaceutical Engineering, School of Chemical Engineering, College of Engineering, University of Tehran, Tehran, Iran

[4]Renewable Energies Department, Faculty of Chemical Engineering, Urmia University of Technology, Urmia, Iran

[5]Department of Chemical Engineering, Tarbiat Modares University, Tehran, Iran

[6]Department of Biomedical Engineering, University Medical Center Groningen, University of Groningen, Groningen, The Netherlands

[7]W.J. Kolff Institute for Biomedical Engineering and Materials Science, University of Groningen/University Medical Center Groningen, Groningen, The Netherlands

[8]Drug Research Program, Division of Pharmaceutical Chemistry and Technology, Faculty of Pharmacy, University of Helsinki, Helsinki, Finland

Correspondence
Sima Rezvantalab, Renewable Energies Department, Faculty of Chemical Engineering, Urmia University of Technology, 57166-419, Urmia, Iran.
Email: s.rezvantalab@uut.ac.ir
Hélder A. Santos and Mohammad-Ali Shahbazi, Department of Biomedical Engineering, University Medical Center Groningen, University of Groningen, Antonius Deusinglaan 1, 9713 AV Groningen, The Netherlands.
Email: h.a.santos@umcg.nl; m.a.shahbazi@umcg.nl

Funding information
Sigrid Jusélius Foundation, the Academy of Finland, Grant/Award Numbers: 331151, 317316; UMCG Research Funds

Abstract

Macrophage targeting and researches centered on immunological responses have received interest thanks to studies unveiling the significant role of macrophages in inflammatory diseases and cancer. In this regard, we have selected four types of nanoparticles (NPs), including acetalated dextran-based nano-carrier functionalized with atrial natriuretic peptide and linTT1(AcDEX-PEG-TT1-ANP), PEGylated acetalated dextran (AcDEX-PEG), acetalated dextran (AcDEX), and hyaluronic acid (HA) to investigate their interactions with macrophage membrane. Using microsecond coarse-grained molecular dynamics (MD) simulations, we studied the interactions between the NPs and the macrophage membrane and subsequent immunological reactions that occur after the penetration of the NPs within the macrophage cell. Different parameters that determine the strength and amount of macrophage membrane interaction were measured and compared for all four types of NPs. The results showed that AcDEX-PEG-TT1-ANP has the most favorable interaction with the macrophage membrane while HA has the least favorable results by comparison. Moreover, drug encapsulation and release in different pH conditions showed the

pH-responsivity of the considered NPs for drug delivery in acidic environments. On the other hand, evaluations with human serum albumin (HSA), fibrinogen (Fib), and transferrin (Tf) declared that peptide modified AcDEX polymers are the most probable NPs to absorb a layer of the protein corona.

KEYWORDS
acetalated dextran, macrophage, molecular dynamics, pH-sensitive release, protein corona

1 | INTRODUCTION

The rapid growth of nanoparticles (NPs) with engineered structure and morphology aims to aid the development of smart materials that can deliver a broad range of therapeutic effects as well as agents that target organs with higher efficiency.[1] Using targeting ligands and stimuli-responsive materials are among various strategies that have been employed for this objective.[2] However critical challenges remain in the way of successful delivery systems such as rapid clearance from the bloodstream, off-target delivery, and even formation of layers of blood proteins around the NPs known as "protein corona". Size control, a layer of polyethylene glycol (PEG)[3] or cell membrane[4] are solutions practiced in the nano-based drug delivery systems to avoid protein corona formation, which is a challenge in targeted drug delivery towards target cells. One of the main targeting attempts that can fail by protein corona formation is the interaction between nanomedicines and immune cells for therapeutic purposes, wherein some life-threatening diseases, such as acute lung injury (ALI), acute respiratory distress syndrome (ARDS)[5] and myocardial infarction,[6] cancer,[7] and so on, immune cells and associated inflammation are highly involved in disease progression. Particularly speaking, macrophages, a significant component of the immune system, have a role in the pathological mechanisms responsible for many diseases, making them a potential therapeutic target for nanomedicines.[8] For example, tumor-associated macrophages (TAMs) have been found abundantly in the tumor microenvironment.[9] The TAMs in the tumor microenvironment help the tumor progression process, leading to metastasis and eventually poor clinical outcomes and survival rates.[10] Therefore, TAMs are specific macrophages that can be targeted by nanomedicines to treat cancer. The goal of this strategy is to reprogram TAMs into anti-tumorigenic macrophages to prevent tumor progression and metastasis.[9] Targeting macrophages also proves to be advantageous for imaging[7a] and diagnostics[11] purposes.

In a process known as macrophage polarization, activated macrophages can mature and turn into two common phenotypes, including M1 pro-inflammatory and M2 anti-inflammatory, in response to molecular clues in their microenvironment.[12] Researchers have proven that STAT1 and IRF5 activation regulates M1 polarization whereas STAT6/STAT3 and IRF4 activation drives macrophages towards M2 polarization.[13] The M1-like macrophages can release pro-inflammatory (interleukin 1 beta, Il1β, TNF-α) and chemoattractants (CXCL3, -8, -10) and play an essential role in the elimination of pathogens, damaged cells, and recruitment of other immune cells to the pathological site. The M1 macrophages might also harm normal cells and attract $CD8^+$T and B lymphocytes to attack the surrounding tissues.[14] That is why inflammation is considered favorable in acute situations and is troublesome in chronic diseases. M2-like macrophages produce anti-inflammatory molecules and growth factors (Il10, TGF-β, VEGF) to control immunity and promote regeneration. At the same time, the abundance of this phenotype is related to a poor prognosis in cancer and infections.[15] In addition, the imbalance between M1 and M2 macrophages is related to several immunity-related diseases. Therefore, therapeutic intervention in this process, to achieve balance, is a potential strategy to alleviate and cure different diseases. For example, strategies used by nano-drugs to target M2 macrophages can be divided into the depletion of TAMs and reprogramming of TAMs.[16] One approach for the depletion of TAMs is the inhibition of colony-stimulating factor 1 receptor (CSF1R) signaling, which plays a role in the apoptosis of a large number of TAMs.[17] Another approach for TAMs' depletion is inhibiting the recruitment of circulating inflammatory monocytes to the tumor site.[7b] As for the reprogramming of TAMs, which is currently one of the most popular approaches for cancer treatment, the reversal of the pro-tumor phenotype into the anti-tumor phenotype is studied.[16,18] By activating the antitumor functions of M1 macrophages and stimulating the activity of Th1 cytotoxic T cells and other effector cells, re-education of TAMs can deactivate the growth of the cancer cells.[19] Targeting small molecules and NPs, such as Toll-like receptor (TLR) agonists, inflammatory cytokines, antibodies, and RNAs for macrophage repolarization have been the focus

of many recent studies.[20] In short, targeting macrophages for anti-cancer therapy can be considered a beneficial approach toward stopping cancer growth.

In addition to cancer therapy by macrophage targeting, Ferreira et al.[21] investigated the in vivo targeting abilities of different heart targeting peptides, concluding that atrial natriuretic peptide (ANP) allow NPs to accumulate in the infarcted heart. However, ANPs suffer from a lack of specificity that prevents them from exclusively targeting cardiac tissue. On the other hand, linear TT1 (Lin-TT1) (AKRGARSTA) has tumor-targeting abilities and confronts tumors by binding to the mitochondrial chaperone protein p32.[22] This protein is usually located inside cells; however, tumor cells, TAMs, tumor endothelial cells, and macrophages associated with atherosclerotic plaques, express them on their surface.[23] Since acetylated dextran (AcDEX) is a biocompatible and pH-responsive polymer, in a recent study, Torrieri et al.[24] also used it as a starting material for the preparation of NPs to target macrophages and treat myocardial infarction. In this work, the nanocarriers were modified with ANP and TT1 peptides to increase their cardiomyocyte targeting abilities. Overall, these AcDEX-based NPs modified with TT1 and ANP were successfully designed and showed promising results. Moreover, HA, as a biocompatible, water-soluble, biodegradable, and non-toxic material with facile chemical functionalization, is considered to be a promising carrier for macrophage targeting[25] through surface receptors, such as CD44, hyaluronan-mediated motility receptor, Toll-like receptor 2 (TLR2), Toll-like receptor 4 (TLR4), and scavenger receptor Stabilin-2 (STAB2)[26] These receptors contribute to HA-mediated macrophage targeting and polarization. An implemented example is plasmid-DNA-encapsulated HA-poly(ethylene imine) NPs designed to modulate macrophage reprogramming.[27] This study concluded that the cytokine-loaded HA particles successfully regulated macrophage polarization toward M2 phenotypes, which can be employed as part of treatment for various autoimmune and inflammation-associated diseases. In another study, Shahbazi et al.[28] used IL-4 encapsulated HA carriers to reprogram macrophage polarization towards M2 phenotypes.

In line with recent studies, we have chosen HA, AcDEX, AcDEX-PEG, and AcDEX-PEG-TT1-ANP as candidates for our MD simulation model.

In the present work, we used a coarse-grained molecular dynamic simulation approach using density functional theory (DFT) simulations to simulate complex systems by an atomistic approach. The interaction of macrophage membranes with NPs as well as the process of adsorption and desorption between nanostructures and macrophages were investigated. In addition, the simulation of corona formation on the NPs is evaluated in deep details.[24] Compared to other molecular and atomic scale studies on macrophage cell membrane interactions,[29] we have selected more biocompatible and efficient nanohybrids to increase the potential of such studies in the clinical translation of nanomaterials. To the best of our knowledge, this is the first study on the molecular evaluation of these NPs with macrophages for drug delivery. In the first part, we have investigated and compared the interaction potency of the four selected NPs with the macrophage cell membrane. In the second stage, we explored the drug loading and release of the selected nanohybrids to exploit the pH-responsive nature of the proposed NP for the enhanced efficiency of drug delivery. In addition, the protein corona formation has been studied as one of the main obstacles for efficient targeting of the above-mentioned nanomaterials.

2 | RESULTS AND DISCUSSION

2.1 | Assessment of the NPs' interactions with macrophage membrane

To better understand the interaction of the NPs with the macrophage membrane, the distribution of the minimum distance between the NPs and the macrophage during the simulations is shown in Figure 1A with snapshots of the last stage of each simulation. As it is shown, the HA has more distance from the macrophage membrane and thus has had little interaction and has subsequently brought the weakest stimulation of macrophages. It can be attributed to the fact that the macrophage membrane consists of multiple hydrophobic lipids while the HA is a hydrophilic polymer. Despite the interaction with the membrane, the polymer collapses with its compartments rather than the membrane surface. It makes the insertion process impossible for the sample due to the steric effect of mass and finally, it ends up at the membrane surface without further penetration. The addition of PEG and PEG-TT1-ANP conjugates to the end of AcDEX makes it amphiphilic and contributes to the interaction of NPs and macrophages. Therefore, the distance between the polymers and macrophages slightly reduces to its minimum in the case of AcDEX-PEG-TT1-ANP.

Assessment of the Rg is a straightforward method to study the interactions in the considered cases.[30] As we know, the smaller the value of Rg, the more compact the macromolecule (Figure 1B). It is noteworthy that the lowest final Rg is related to the AcDEX-PEG-TT1-ANP system. The difference between final and initial Rg presented as ΔRg is a more critical point in the evaluation of the efficacy of the NPs and can be interpreted as a scale of compactness and agglomeration for the considered cases. A reduction in the ΔRg with the introduction of PEG and PEG-TT1-ANP

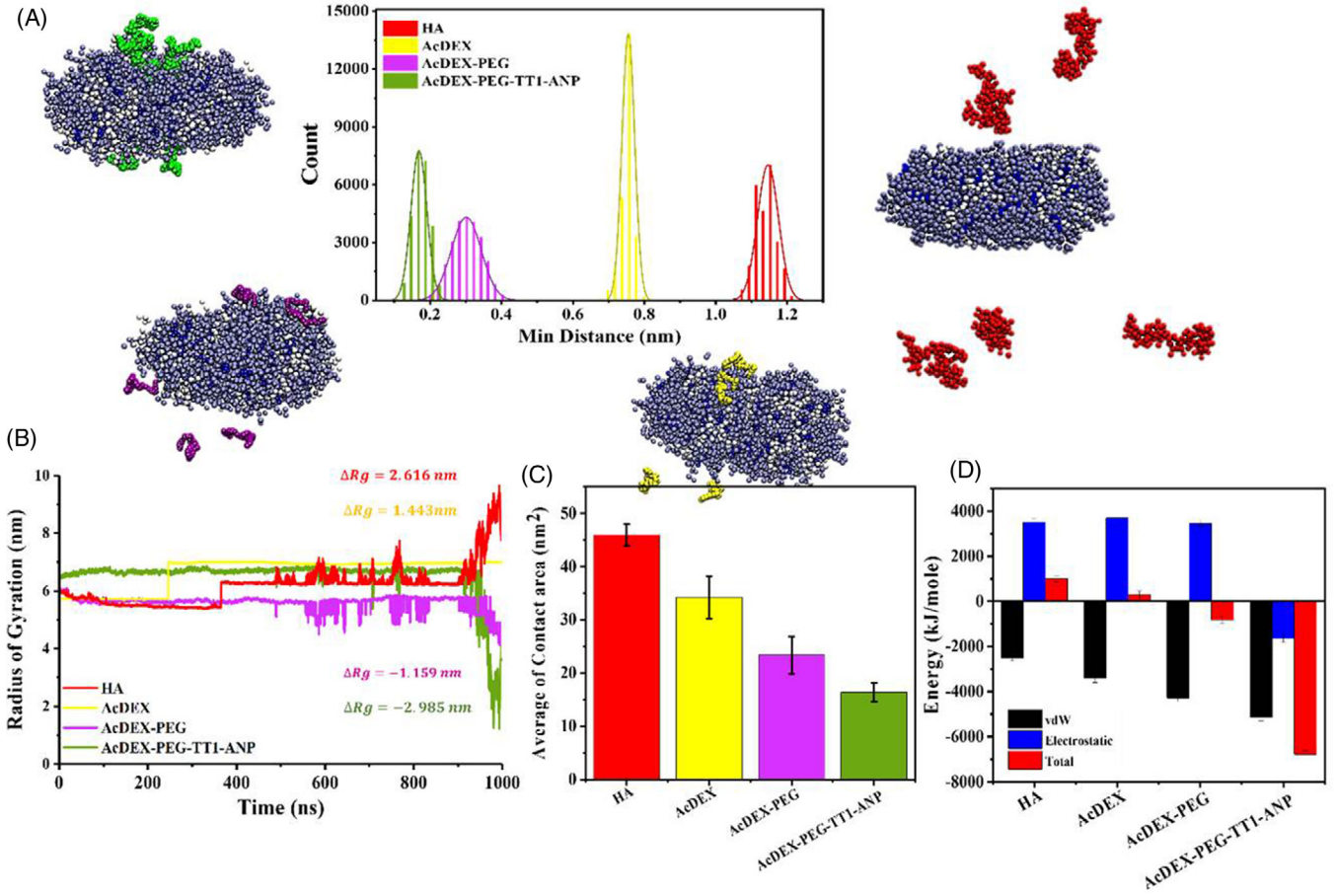

FIGURE 1 (A) The distribution of the average minimum distance of the NPs and macrophages during 1-microsecond simulation. Snapshots of the simulations are provided on each diagram to offer a better understanding of the minimum distance between the total mass of polymers with macrophages. (B) Variation of Rg for each simulation on the course of interactions. (C) Average contact area for polymers that clearly shows the reduced contact area of AcDEX-PEG-TT1-ANP due to the adsorption on the surface of the macrophage. (D) Energy analysis of the interactions of polymers with macrophage

segments to the AcDEX was observed. These findings are in line with the study of Gu et al.[29] who claimed PEGylation of nanoflakes enhances the affinity of NPs toward macrophages. As it is apparent, the most integrated structure belongs to AcDEX-PEG-TT1-ANP which is in favor of its macrophage stimulation properties and responses.

We also evaluated different parameters related to the interaction between these NPs and the macrophage membrane, comparing them in terms of efficacy and response initiated within the macrophage. The average contact area between a group of NPs' molecules within themselves is shown in Figure 1C. HA shows the highest value that indicates the HA molecules are more drawn to each other and tend to interact by themselves rather than the macrophage membrane. The contact area decreased in AcDEX and AcDEX (in the order stated) as the least amount of average contact area is presented by AcDEX-PEG-TT1-ANP, revealing its tendency to interact with the macrophage membrane. Therefore, in agreement with previous results, AcDEX-PEG-TT1-ANP has the most rate of interaction, and HA has the least.

The interaction of NPs with macrophages was also assessed from the energetic point of view. Both the bond type and the amount of interaction energy are significant factors for molecular interactions. To analyze the nature of the observed interactions, the constituents of the total energy vectors were inspected. In particular, van der Waals (vdW) and electrostatic forces have been considered as the main determinant forces in the attraction and repulsion of the particles. In this regard, Figure 1D represents vdW and electrostatic energies and respective total energy for the interaction between each nanohybrid and the macrophage membrane as their average values throughout simulations. According to the graph, AcDEX-PEG-TT1-ANP has the most amount of vdW energy followed by AcDEX-PEG, AcDEX, and then finally HA. Among all the carriers, HA has the least vdW attraction

and the most electrostatic repulsion with the membrane. The negative charge of the HA causes an electrostatic repulsion between it and the macrophage membrane. In the case of poor vdW interaction between HA and membrane, hydrophobicity of the HA should be noted. HA has hydrophilic nature while AcDEX and its derivatives are amphiphilic and have hydrophobic parts in their structures that can promote vdW interactions with hydrophobic lipids of the macrophage membrane. In accordance with results presented by Söldner et al.,[31] the vdW energy increases with an increased chain length of interacting groups. Similar results are observed for AcDEX, AcDEX-PEG, and AcDEX-PEG-TT1-ANP in which polymers with longer chain lengths have stronger vdW and consequently stronger total energy interactions. Ultimately, it can be easily found that the modification of dextran with hydrophobic groups boosts its performance in the stimulation of macrophages. It is concluded that the modification of AcDEX promotes vdW and electrostatic interactions with macrophages and AcDEX-PEG-TT1-ANP could make the strongest and most efficient bonds with the cell membrane, indicating its competence to deliver its cargos to the targeted macrophages.

The electrical charge of NPs was examined in the aqueous medium. HA loses one hydrogen per monomer, and as a result, its conjugated base has a negative charge per monomer. AcDEX also loses one hydrogen per monomer in the aqueous medium and acquires a negative charge per monomer. Because the AcDEX monomer has more atoms compared to the HA monomer, the charge to surface ratio of each AcDEX monomer is lower than that of HA. The introduction of PEG segments to AcDEX monomer, increases the number of atoms and consequently the surface of monomers in comparison to the AcDEX monomer. The addition of LinTT1 peptide (with neutral charge) to the monomers only increases the size of the molecule. In the aqueous medium, the charge of ANP peptide is equal to four. Therefore, the addition of these two peptides to the AcDEX-PEG changes the charge of molecule (AcDEX-PEG-TT1-ANP) to +2. Negatively charged macrophage membrane attracts the AcDEX-PEG-TT1-ANP NP, while there is a negative repulsive force between the macrophage and AcDEX-PEG, AcDEX, and HA NPs. Among NPs with negative charge, NPs that have a higher charge to surface ratio will have a greater repulsive interaction with macrophage membrane, and vice versa. Altogether, we predict that the macrophage membrane is inclined to attract the AcDEX-PEG-TT1-ANP NPs, eliciting subsequent macrophage activation and immune responses. Also the repulsive force between the membrane and other mentioned particles will be as follows HA > AcDEX > AcDEX-PEG. The main repulsion factor was electrostatic energies due to the homonymous charge of NPs, and the adsorption was associated with vdW energies and the ratio of charge to surface. Interestingly, the addition of PEG polymer changes the charged surface of AcDEX NPs toward less interaction with macrophages, and the addition of this molecule to AcDEX also increases the vdW energies. These results can be seen well in Figure 1D. The total energy between the two NPs and the macrophage changed from positive to negative due to the reduction of the charge to surface ratio in the AcDEX-PEG NPs.

RMSD reflects the fluctuations of the particle calculated at different points of the simulation time relative to a constant reference. The smaller the RMSD values, the more stability of the system and hence, better interactions between the NPs and the macrophage cellular membrane. The greater the oscillations of the particles, the more unstable the system, and the greater the slope of the RMSD will be.[32] Figure 2A,B depict the maps of the Rg variation versus RMSD fluctuations for HA and AcDEX-PEG-TT1-ANP, respectively. As it is clear, the interaction of HA polymer with macrophage led to an extended Rg level in a broad range of RMSD fluctuations. For the latter case, the Rg variations are less in comparison with other samples; however, it is not in the favor of interactions. The absolute values of Rg are high, which indicates the weakest attraction of the polymer chains toward the macrophage. Conjugation of PEG chains to the polymer strands improves the interactions where the Rg values drop to the lowest level among other peers. It indicates that PEGylation can significantly improve the attraction of polymer to the macrophage. Furthermore, the introduction of peptides (TT1 and ANP) enhances the stimulation of macrophages since the RSMD oscillation 3.5 nm to 5 nm range is between is noticed monitored for the NPs containing conjugated peptides (Figure 2A).

The interaction and even insertion of NPs in the macrophage are largely determined by energy and enthalpy calculations. However, we came up with the idea of whether the entropy of transferring the polymer strands can be effective in the whole process. The coarse-grain and atomistic models predict enthalpic origins of the phenomena whereas principal component analysis (PCA) calculates the atomic coordinates, determining the distribution of positions in space within the simulated model. The simulation (using gmx anaeig code) computes entropy based on the Quasiharmonic approach and based on Schlitter's formula. Figure 2C illustrates the entropic analysis of the phenomena. PCA data analysis (positioning of the atoms and the 2D trajectories) shows that the atoms within the AcDEX-PEG-TT1-ANP simulation were relatively compressed and compact throughout the simulation box. The distribution of atoms becomes more dispersed with AcDEX-PEG, this pattern continues with AcDEX and finally, HA demonstrated the most dispersed

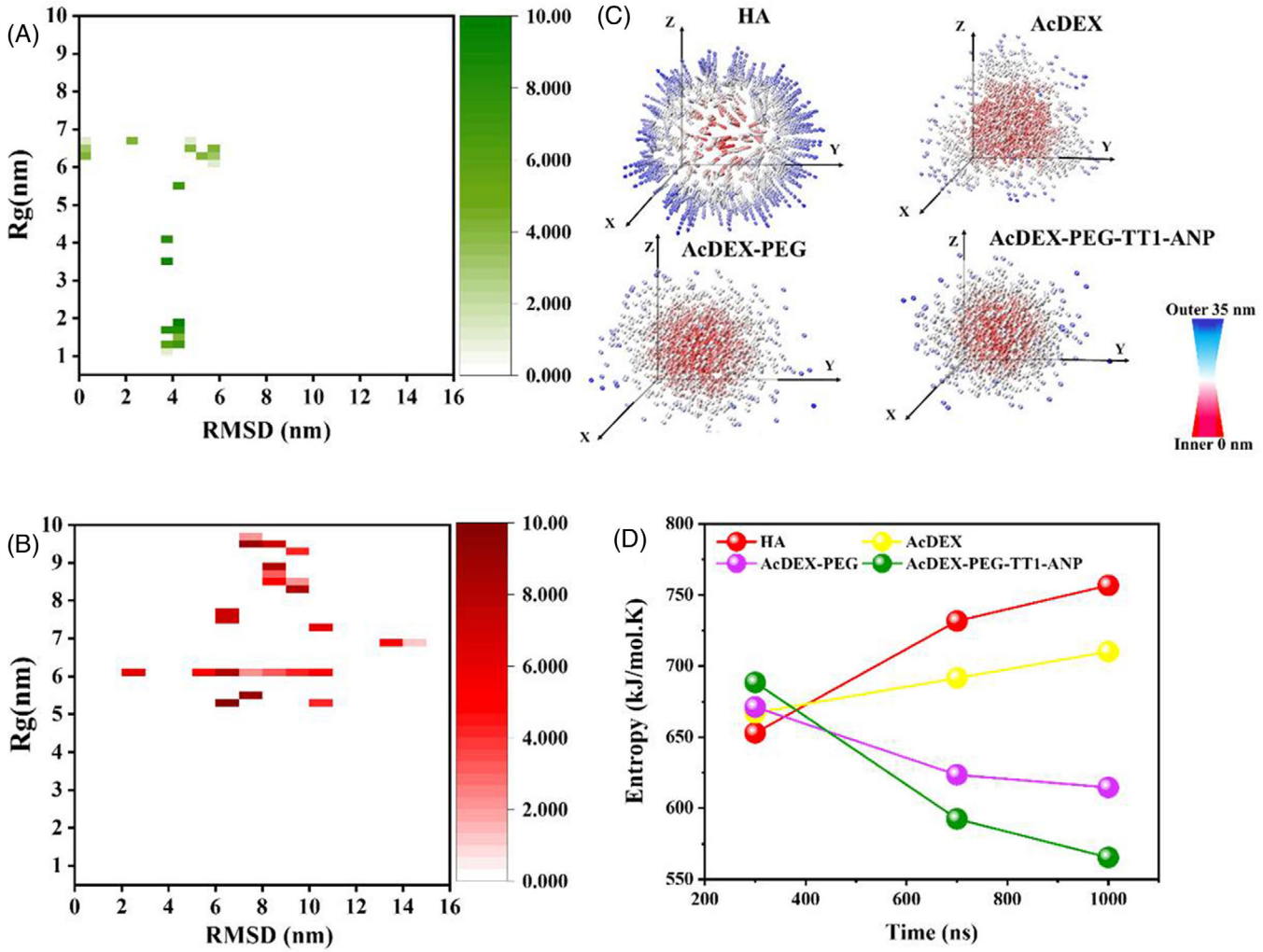

FIGURE 2 (A, B) The map of the Gyration radius (Rg) versus Root-Mean-Square-Deviation (RMSD) fluctuations for AcDEX-PEG-TT1-ANP and HA, respectively. Accumulation of points at lower RMSDs and lower Rgs indicates less fluctuations and smaller size for the simulated NPs, which could indicate system stability. (C) Principle component analysis (PCA) of the interaction of NPs and macrophages. This is a three-dimensional expression of entropy in the simulation box space. In this diagram, the higher the density in the inner region, the more accumulated the molecules are. The higher the density in the outer region, the more dispersed the molecules are. (D) The entropy of the interactions of macrophage with NPs. A decrease in entropy over time can indicate a reduction in system fluctuations and that the system is moving towards an optimal state

and least compact set of atoms within the simulation box. Compact atoms and compression point to better interaction between the atoms, meaning better interaction between the nanohybrid and macrophage cell membrane. That brings us to the conclusion that AcDEX-PEG-TT1-ANP can settle on the macrophage by comparison in this analysis and AcDEX-PEG, AcDEX and HA follow suit in order. Figure 2D displays the entropy calculated for each polymer at 3 different points in time. The more the entropy calculated within the simulation timeframe decreases, the more accumulation is seen and suspected within the polymer membrane structure leading to a better macrophage stimulation and subsequent response. Therefore, the best response is displayed by AcDEX-PEG-TT1-ANP and the least favorable response, by comparison, is displayed by HA. AcDEX-PEG and AcDEX have the second and third best responses, respectively. According to the graph, AcDEX-PEG-TT1-ANP showed the most decrease in initial entropy value, 1000ns within the simulation, having AcDEX-PEG and AcDEX as the next ones. However, HA demonstrated increased entropy.

In an overall view, by examining the data acquired from the simulation and analyzing the parameters measured throughout the process, we have concluded that AcDEX-PEG-TT1-ANP establishes a strong interaction with the cell membrane of the macrophage. HA had the weakest cell membrane interaction in the lineup. These findings point to the fact that AcDEX is a more efficient starting structure

compared to HA in macrophage membrane targeting and also it must be noted that functionalizing nanocarriers or NPs with peptides could increase the infiltration and penetration ability of these NPs within the cell membrane.

Our simulation approved the experimental data acquired in the study conducted by Torrieri et al.,[24] Compared to MoS_2 nanoflakes that were also studied on an atomistic scale,[29] our tested NPs prove to have similar interaction potential and subsequent macrophage stimulation potency. Considering that the selected NPs are superior in biocompatibility measures, they would be more favorable in a clinical seTT1ng.

2.2 | Drug loading and release evaluations

As the next step for the evaluation of selected NPs, we have simulated the pH dependency of drug loading and release from NPs. In accordance with Torrieri et al., in the new mathematical model, two hydrophobic drugs, CHIR99021 (CHIR) and SB203580 (SB) were separately loaded into NPs and their release profiles were tested. It should be mentioned that to have wet lab conditions, polyvinyl alcohol (PVA) (a stabilizer of emulsion) is also considered in the compositions. Afterward, drug loading and release were investigated in two pH values of 7 and 5 in phosphate buffer saline (PBS) and acetate buffers. Among all simulations, the AcDEX-PEG-TT1-ANP NPs displayed stronger vdW attraction with drug molecules at pH 7 as they have lower energy levels (Figure 3A-i). On the other side, the AcDEX-PEG-TT1-ANP NPs represented electrostatic repulsion (Figure 3A-ii) with drug molecules. The observations can be attributed to the hydrophobic-hydrophobic attractions of NPs' components.[33] HA-based NPs possessed the strongest electrostatic attractions with both drugs, regardless of the pH of the medium. Attraction energies have negative sign, so when attraction energy increases, the energy has a lower level (most negative). AcDEX-PEG-TT1-ANP NPs have less attraction energy with drug molecules (Figure 3A-iii) when compared with HA and AcDEX-PEG NPs. It indicates the most successful drug loading for HA, especially at pH 7. Because in this pH, HA-drug attraction energy is most negative compared to other carriers. The presence of TT1-ANP on the surface of AcDEX-PEG NPs turns it to the least successful NPs in drug loading among the studied cases.

The stability of NPs could be measured from Gibbs free energy as the absolute criteria of stability. The diagram in Figure 3B represents the release and energy level for the individual cases. According to the diagram, regardless of drug type, NPs have a lower level of energy at pH 7, that is, they tend to keep the drug compounds in their structures. At acidic pH, stability decreases, and NPs begin to release the payload. Considering the drug type, it can be seen that at basic pH CHIR-loaded NPs is more stable; however, at basic pH, SB-loaded NPs have a stronger complex. Interestingly, the observations are in excellent agreement with experimental findings[24] that at pH 5, CHIR has higher solubility and a tendency to get released into the surrounding media. Therefore, we can categorize the diagram into release and loading sections at acidic and basic pH, respectively. The release results at the end of the simulation are in good agreement with experimental observations as SB-loaded NPs show a higher release amount regardless of pH conditions.

Snapshots in Figure 3C exhibits the structures of HA- and AcDEX-PEG-TT1-ANP- based NPs loaded with CHIR at pH 7. All the simulation-wise observations are in good agreement with the previous empirical findings[32,34] on the pH-responsive nature of the AcDEX-based[35] and HA-based[36] NPs. Moreover, drug release from AcDEX-based NPs can be controlled based on the ratio of cyclic and acyclic acetal groups present in the structure.[37] Surface modification of the AcDEX with PEG-TT1-ANP groups facilitates the drug release at acidic conditions as it is shown that AcDEX-loaded NP releases only 60% and 55% of its CHIR and SB payload, respectively, in 1 μs timespan while the release increased up to 100% and 95% when the polymer is conjugated by peptide groups. Strikingly, the addition of only PEG groups reduced the release of NPs while modification of the AcDEX with PEG-TT1-ANP promoted the drug release.

Also, the charge of the molecules can well indicate the main reason for the adsorption and repulsion of the drugs to the NPs. The AcDEX-PEG-TT1-ANP nanoparticle, which is positively charged due to the addition of the ANP molecule, has repelled drugs. At acidic pH, AcDEX-PEG-TT1-ANP nanoparticle and drugs are more positively charged and cause more electrostatic repulsion. These homonymous and non-homonymous charges have clearly caused the NPs to be closer or farther apart. In fact, the electrostatic repulsion and adsorption has caused the NPs to move farther or closer to each other. Lennar Jones energy has caused more or less vdW energy and it directly correlates with the distance between NPs and drugs. The sum of vdW and electrostatic energies also shows the total energy, which is the main factor of adsorption and repulsion. In fact, the higher total energy results in the higher intensity of NPs' adsorption and vice versa. Based on the explanations provided, we can clearly see that lower Gibbs free energy and higher adsorption percentage are for HA NPs and drugs, and higher Gibbs free energy and lower adsorption percentage are for AcDEX-PEG-TT1-ANP and drugs, confirming the explanation related to the homonymous and non-homonymous charges of NPs.

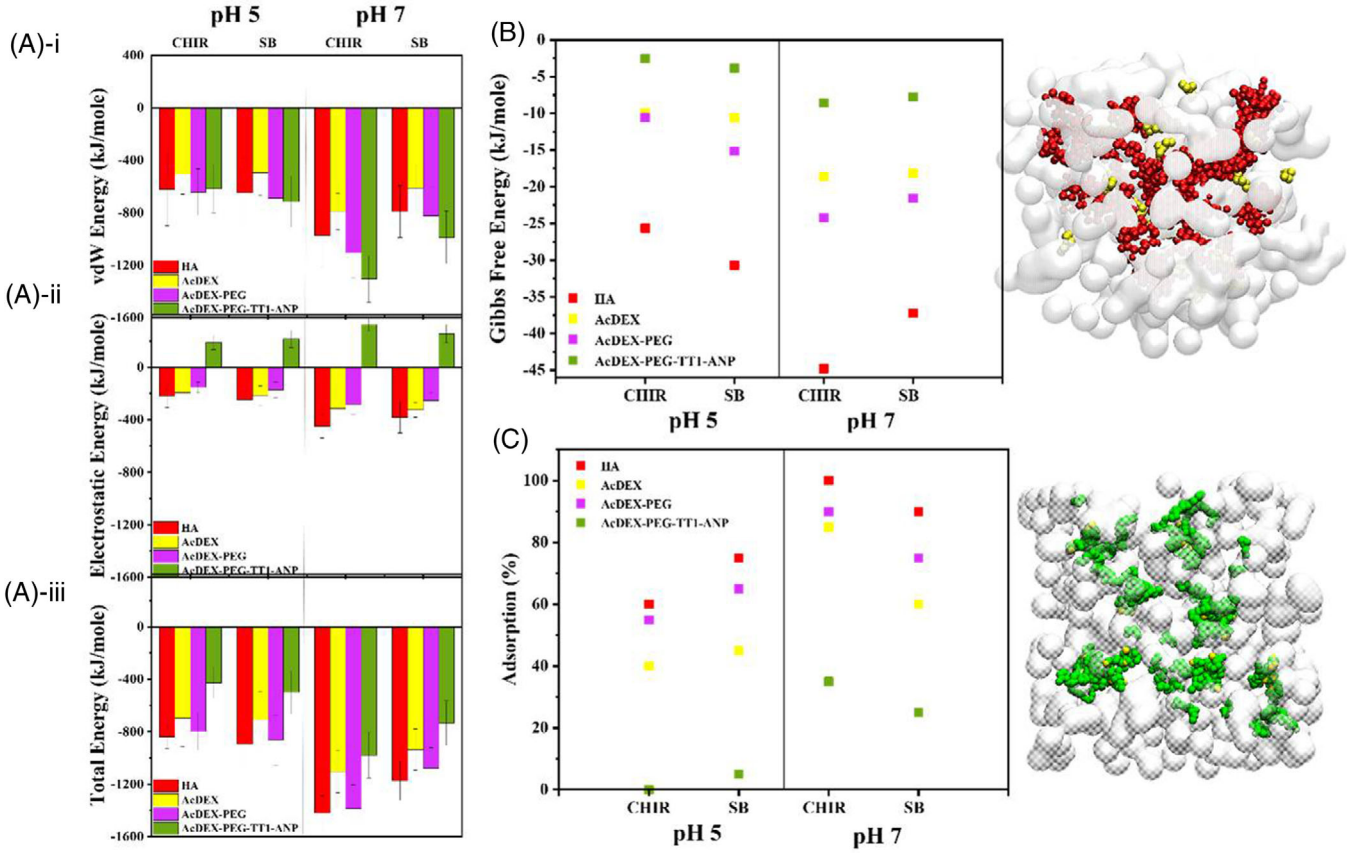

FIGURE 3 The evaluations of drug loading and release. (A-i-iii) Energy analysis (vdW, electrostatic, and total energy) of NPs indicates that at pH 7, drugs are strongly attracted to the nanosystem while at pH 5 the complexes have higher energy levels as an indicator of their tendency to release the drug molecules. (B) The results of Gibbs free energy calculations and pH dependency of drug loading. (C) The pH-dependent adsorption of drug molecules on the NPs. Snapshots of drug-loaded polymers represent a visual understanding of the adsorption levels. PVA, HA, and AcDEX-PEG-TT1-ANP strands are silver, red, and green molecules, respectively. CHIR drug molecules are small yellow spheres that are visible in the HA-based NPs while few CHIR molecules are loaded in the AcDEX-PEG-TT1-ANP NPs

2.3 | Investigation of corona formation on NPs

Protein corona formation around the NPs can affect the efficacy of delivery systems.[38] Computational methods are powerful tools for the evaluation of coronal formation phenomena on various NPs.[39] In this section, the effect of three abundant blood proteins, including human serum albumin (HAS), transferrin (Tf), and fibrinogen (Fib) are investigated in the formation of the protein corona around NPs. To this end, the polymers are placed with individual proteins and their interactions are monitored for 1 μs. Figure 4A represents the energy of the interactions between NPs with blood proteins. In a bird-eye-view, it can be understood that HA and AcDEX polymers show no tendency toward the three blood proteins. As it is clear, electrostatic repulsion is responsible for the observed results, which stem from the net negative surface charge of the tested three proteins.[40] It should be mentioned that vdW attractions have very small contributions to the total energies, in all cases. However, the presence of PEG chains promotes the interaction of the polymers with blood proteins where proteins are more attracted to the surface of the AcDEX-PEG. It has been stated that the PEG molecules are likely to interact with hydrophobic residues.[41] In this sense, the introduction of PEG structures increases the tendency of polymers toward hydrophobic residues of proteins. Furthermore, the addition of the -TT1-ANP shifts the polymers' charge toward positive values and promotes the attraction of AcDEX-PEG-TT1-ANP with stronger electrostatic and consequently total energies to the surface of all three proteins.

On the other hand, among the three proteins, the Fib is more likely to be absorbed on the surface of NPs, which has stronger energy values with them. Notably, Fib repels HA strand stronger in comparison with other proteins. Therefore, it can be understood that Fib has stronger interactions with polymers. Our findings are in good agreement with

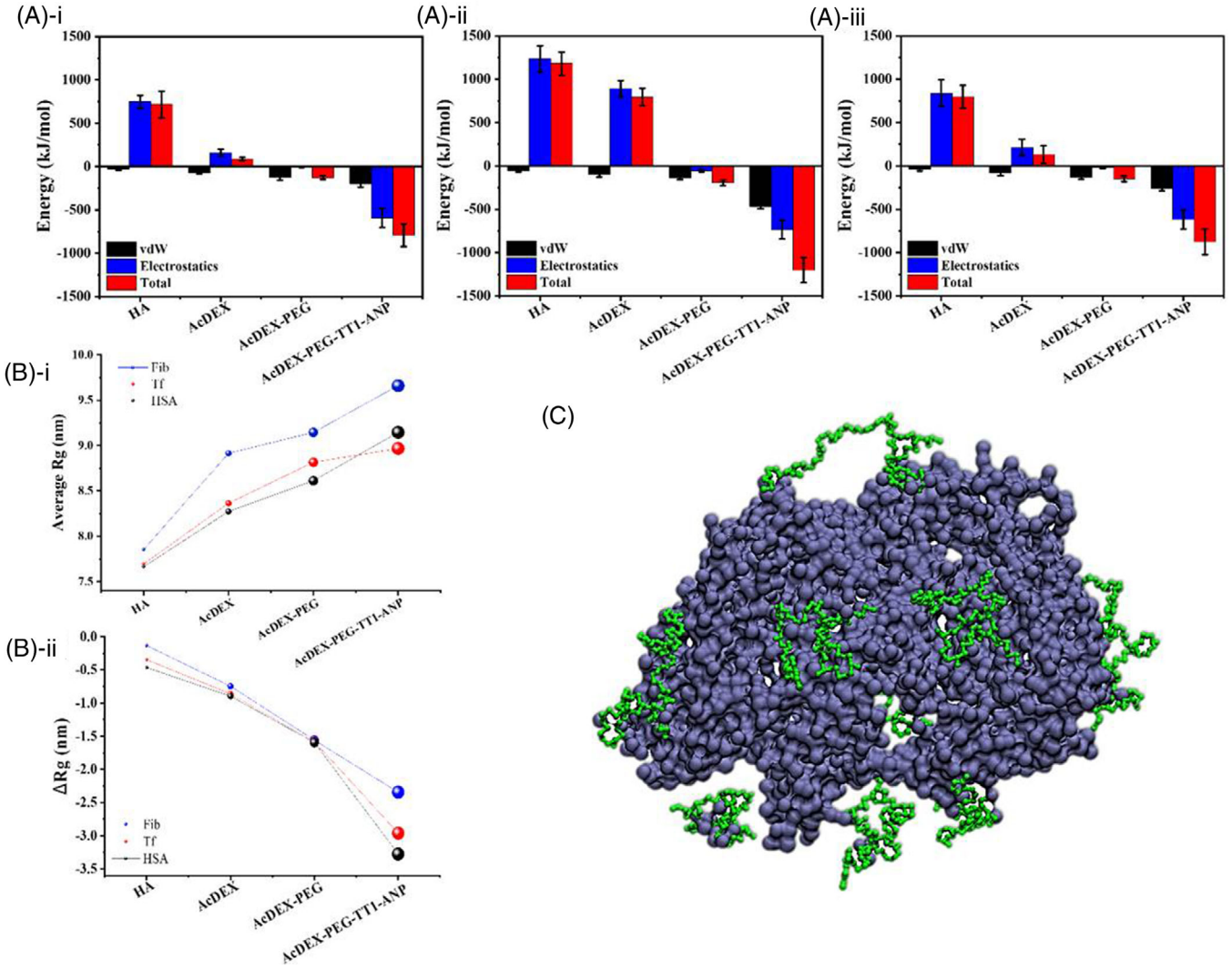

FIGURE 4 (A) The interaction energy of HSA, Fib, and Tf with the NPs, respectively. (B-i,ii) The average Rg and ΔRg simulation systems consisted of blood proteins in the presence of the NPs. (C) The snapshot of the attraction of AcDEX-PEG-TT1-ANP strands on the surface of HAS, indicating the strong interaction of the polymers with protein corona to be formed around the NPs

Vilanova et al.[42] as they predicted that in the long run, Fib succeeds the competition with the other two proteins and covers the NPs' surfaces. Although our simulations are carried out individually, the results provide more insights into the competitive nature of the proteins' adsorptions on NPs surfaces. Tavanti et al.[43] suggested that due to its structure and geometry, Fib has plural binding sites, which can contribute to the stronger interaction of Fib macromolecules with the polymers.

According to Azman et al.,[44] Rg and ΔRg give insights into the corona formation around NPs. Therefore, to deeply explore the outcomes, the dynamic of corona formation is evaluated in terms of Rg and ΔRg regarding polymer strands and blood protein in the course of the simulation and the behavior that the substances show in the blood environment and their accumulation in this simulation are quite similar to the simulation with respect to Rg and ΔRg. The smaller the Rg size for the whole simulation box, the larger the attraction among the proteins and polymers. Rg reduces to much lower values than its initial values in the presence of AcDEX-PEG-TT1-ANP compared with other polymers, especially HA polymers. To better understand the conformational change of the systems due to the movement of molecules toward or away from each other, ΔRg was computed as the difference in the initial and final Rg values (initial value- final value). The larger the ΔRg, the longer the path have been taken toward each other during the time period. The greater the changes in the initial point Rg compared to the final point, the greater the equilibrium in the system The AcDEX-PEG-TT1-ANP NPs show the highest stability and this depends on the greater uptake of these NPs than other NPs. That is, there has been more accumulation. The small observed values also can be attributed to the conformational changes of individual

molecules due to the equilibration. Figure 4C reflects the visual insight on the aggregated AcDEX-PEG-TT1-ANP polymers around the Fib that clearly shows the multiple binding sites for the polymers with the protein structure.

3 | CONCLUSIONS

In this study, we created a MD model to examine the interaction between four distinct NPs and the macrophage membrane, and also evaluated the macrophage stimulating potential of each NP. The AcDEX-PEG-TT1-ANP has shown the most suitable criteria for drug delivery through analyzing different parameters, including interaction energies, entropy, stability, compactness, the distance between the NPs and the membrane, and contact area. According to the results, AcDEX-PEG-TT1-ANP is retained on the macrophage membrane more than those of the other selected structures, leading to a better immunological response and cytokine stimulation.

Next, using two different drug types, the pH-responsive drug loading and release are proven for all NPs. In this sense, all polymers release their payload in the acidic conditions that can be utilized in the delivery to acidic environments, such as tumor cells. Although the computed loading capacity at pH 7 is the lowest for AcDEX-PEG-TT1-ANP among its peers, it can completely release drug molecules. On the other hand, HA has the highest loading and lowest release rate at acidic and basic environments, respectively.

Finally, blood protein corona formation was studied using three abundant proteins, namely HAS, Fib, and Tf. The study demonstrated that due to the positive surface charge of the AcDEX-PEG-TT1-ANP, it could attract more proteins on its surface. Contrarily, HA exhibit the least interaction with all three blood protein types.

Considering the many possible therapeutic applications of macrophage targeting by nanomaterials, this study could be a cornerstone for further design of targeted drug delivery systems that can be beneficial for the treatment and diagnosis of many inflammatory diseases and cancers. MD can assist in accelerating and simplifying the process. The limitations of MD studies are insufficient or lack of experimental data to back up the results on a larger scale. In this study, we have investigated functionalized NPs that were previously examined through experimental approaches in a novel study, and insufficiency in experimental data has decreased. Our MD study has allowed better identification of suitable nanomedicines for therapeutic application; however, further in vivo studies still need to be conducted to give us more supportive experimental reliable data for the bench to bedside transition of nanomaterials.

4 | SIMULATION SECTION

4.1 | Detail of simulations

In this work, coarse-grained simulations were performed using the martini force field. The macrophages were parameterized by Python scripts located on the Martini website. Other molecules were also manually parameterized with bids that were found on the Martini website based on their All-Atom model. The electrostatic potentials were calculated via DFT simulation on the All-Atom model. The parameterization of the molecules at different pH levels was achieved by changing the particle charge in their topology files. Subsequently, the new molecules were defined using the Avogadro software. This was done by Epsilon and Sigma values provided by the martini website and the information imported from the topologies of each molecule. Thereafter, the molecules designed by the Martini Force Field were compared with the molecules designed in the All-Atom model. An All-Atom simulation and a coarse-Grained simulation were both applied to each molecule, and the Martini topology data was modified according to the All-Atom simulation data. Additionally, All-Atom simulations were performed with the OPLS-AA force field, and molecules were also parameterized using the polypargen website. After matching the Martini force field data and the All-Atom data, the molecules were ready for simulation. The CHIR99021 (CHIR) and SB203580 (SB) were designed by Avogadro software and optimized by DFT method using B3LYP and their electrostatic potentials (ESP) charges was calculated. Then, Coarse Grained model was designed by Avogadro software and the obtained charges were entered in their topology.

The polar water model on the Martini website was used for the simulations. The length of the cubic box was 35 nm. The simulation box ran for 1 μs with a 20 fs time step. Parrinello-Rahman barostat and nose hoover thermostat algorithms were employed to couple the ambient temperature and pressure. At the end of the simulation, the minimum distance, contact area, energy, radius of gyration (Rg), Root-Mean-Square-Deviation (RMSD), entropy, Gibbs free energy, and adsorption were analyzed for different modes. These analyses were achieved using the commands gmx mindist, gmx sasa, g_mmpbsa, gmx gyrate, and gmx rmsd. The Charges of simulated molecules and NPs are presented in Table 1.

4.2 | Macrophage manufacturing process

The membrane of macrophages is composed of cholesterol 35.00%, POPC 28.15%, sphingomyelin 10.27%, POPE

TABLE 1 The charges of the different components and NPs at neutral and acidic pH values

Molecule	Charges	
	pH 7	PH 5
HA	−2	0
AcDEX	−2	0
AcDEX-PEG	−2	0
AcDEX-PEG-TT1-ANP	2	4
CHIR drug	1	2
SB drug	1	1

TABLE 2 Percentages, numbers, and charges of each lipid in the macrophage

Lipids of macrophage	Number of lipid molecules in macrophage	Percent of lipids in macrophage	Charges
Cholesterol	136	35	0
POPC	110	28.1	0
Sphingomyelin	40	10.3	0
POPE	38	9.8	0
POPG	30	8	−1
POPI	20	5.5	−1
POPS	12	3.3	−1

9.75%, POPG 8.00%, POPI 5.53%, POPS 3.32%. These lipids are composed of 136, 110, 40, 38, 30, 20, and 12 molecules, respectively.[29] Lipid structures were designed with a square area of 11 nm × 11 nm in the Martini force field using Charmm_GUI (https://www.charmm-gui.org/). However, another way to design them is the Python scripts provided on the Martini Force Square site (http://cgmartini.nl/). The topologies provided in the Lipid section of Martini's site were also used. The molecules were simulated and optimized in an 18 nm cube box of 400 ns in 25 fs time steps. The polar water type of the Martini force field was used to optimize the macrophage. The algorithms and optimization methods were performed as in the steps described in Section 4.1. Also the details of the macrophage, which include the charge as well as the percentage and number of each lipid, are provided in the Table 2.

ACKNOWLEDGMENTS

Financial support from the Sigrid Jusélius Foundation, the Academy of Finland (grant nos. 331151 and 317316), and the UMCG Research Funds is acknowledged. The authors thank Fatemeh Alimohammadi for her assistance during the data analysis of this study.

CONFLICT OF INTEREST

The authors declare no conflict of interest.

DATA AVAILABILITY STATEMENT

The data presented in this study are available on request from the corresponding author.

ORCID

Hélder A. Santos https://orcid.org/0000-0001-7850-6309

REFERENCES

1. T. Lammers, M. Ferrari, *Nano Today* **2020**, *31*, 100853.
2. a) W. Cui, J. Li, G. Decher, *Adv. Mater.* **2016**, *28*, 1302; b) Y. Lu, A. A. AimeTT1, R. Langer, Z. Gu, *Nat. Rev. Mater.* **2016**, *2*, 1.
3. J. S. Suk, Q. Xu, N. Kim, J. Hanes, L. M. Ensign, *Adv. Drug. Deliv. Rev.* **2016**, *99*, 28.
4. C.-M. J. Hu, L. Zhang, S. Aryal, C. Cheung, R. H. Fang, L. Zhang, *Proc. Natl. Acad. Sci.* **2011**, *108*, 10980.
5. A. Dushianthan, M. Grocott, A. Postle, R. Cusack, *Postgrad. Med. J.* **2011**, *87*, 612.
6. M. Jung, M. Dodsworth, T. Thum, *Basic Res. Cardiol.* **2019**, *114*, 4.
7. a) S. Mukherjee, D. Sonanini, A. Maurer, H. E. Daldrup-Link, *Theranostics* **2019**, *9*, 7730; b) Y. Jin, G. Hu, M. Guo, J. Xu, F. Wu, J. Fan, Q. Huang, G. Yang, Z. Lv, X. Wang, *Front. Immunol.* **2019**, *10*, 1998.
8. S. Wang, R. Liu, Q. Yu, L. Dong, Y. Bi, G. Liu, *Cancer Lett.* **2019**, *452*, 14.
9. J. Li, D. J. Burgess, *Acta Pharmaceutica Sinica. B* **2020**, *10*, 2110.
10. E. Muntimadugu, N. Kommineni, W. Khan, *Pharmacol. Res.* **2017**, *126*, 109.
11. A. Aalipour, H.-Y. Chuang, S. Murty, A. L. D'Souza, S.-m. Park, G. S. Gulati, C. B. Patel, C. Beinat, F. Simonetta, I. Martinić, *Nat. Biotechnol.* **2019**, *37*, 531.
12. a) M. S. Dukhinova, A. Prilepskii, A. A. Shtil, V. V. Vinogradov, *Nanomaterials* **2019**, *9*, 1631; b) L. Wang, H. Zhang, L. Sun, W. Gao, Y. Xiong, A. Ma, X. Liu, L. Shen, Q. Li, H. Yang, *J. Nanobiotechnol.* **2020**, *18*, 1.
13. F. R. D'Alessio, J. M. Craig, B. D. Singer, D. C. Files, J. R. Mock, B. T. Garibaldi, J. Fallica, A. Tripathi, P. Mandke, J. H. Gans, *Am. J. Physiol. Lung Cell Mol. Physiol.* **2016**, *310*, L733.
14. a) B. Bogen, M. Fauskanger, O. A. Haabeth, A. Tveita, *Cancer Immunol. Immunother.* **2019**, *68*, 1865; b) A. Carestia, H. A. Mena, C. M. Olexen, J. M. O. Wilczyñski, S. Negrotto, A. E. Errasti, R. M. Gómez, C. N. Jenne, E. A. C. Silva, M. Schattner, *Cell Rep.* **2019**, *28*, 896.
15. A. Boissonnas, M. Laviron, *Front. Immunol.* **2019**, *10*, 1799.
16. D. G. DeNardo, B. Ruffell, *Nat. Rev. Immunol.* **2019**, *19*, 369.
17. S. M. Pyonteck, L. Akkari, A. J. Schuhmacher, R. L. Bowman, L. Sevenich, D. F. Quail, O. C. Olson, M. L. Quick, J. T. Huse, V. Teijeiro, *Nat. Med.* **2013**, *19*, 1264.
18. M. Ovais, M. Guo, C. Chen, *Adv. Mater.* **2019**, *31*, 1808303.
19. C. D. Mills, L. L. Lenz, R. A. Harris, *Cancer Res.* **2016**, *76*, 513.
20. F. J. Van Dalen, M. H. Van Stevendaal, F. L. Fennemann, M. Verdoes, O. Ilina, *Molecules* **2019**, *24*, 9.
21. M. P. Ferreira, S. Ranjan, A. M. Correia, E. M. Mäkilä, S. M. Kinnunen, H. Zhang, M.-A. Shahbazi, P. V. Almeida, J. J. Salonen, H. J. Ruskoaho, *Biomaterials* **2016**, *94*, 93.
22. S. Sharma, V. R. Kotamraju, T. Mölder, A. Tobi, T. Teesalu, E. Ruoslahti, *Nano Lett.* **2017**, *17*, 1356.
23. a) L. Paasonen, S. Sharma, G. B. Braun, V. R. Kotamraju, T. D. Chung, Z. G. She, K. N. Sugahara, M. Yliperttula, B. Wu,

M. Pellecchia, *ChemBioChem* **2016**, *17*, 570; b) J. Hamzah, V. R. Kotamraju, J. W. Seo, L. Agemy, V. Fogal, L. M. Mahakian, D. Peters, L. Roth, M. K. J. Gagnon, K. W. Ferrara, *Proc. Natl. Acad. Sci.* **2011**, *108*, 7154; c) V. Fogal, L. Zhang, S. Krajewski, E. Ruoslahti, *Cancer Res.* **2008**, *68*, 7210.

24. G. Torrieri, F. Fontana, P. Figueiredo, Z. Liu, M. P. Ferreira, V. Talman, J. P. Martins, M. Fusciello, K. Moslova, T. Teesalu, *Nanoscale* **2020**, *12*, 2350.
25. a) S. Mizrahy, S. R. Raz, M. Hasgaard, H. Liu, N. Soffer-Tsur, K. Cohen, R. Dvash, D. Landsman-Milo, M. G. Bremer, S. M. Moghimi, *J. Controlled Release* **2011**, *156*, 231; b) J. E. Rayahin, J. S. Buhrman, Y. Zhang, T. J. Koh, R. A. Gemeinhart, *ACS Biomater. Sci. Eng.* **2015**, *1*, 481.
26. a) D. Jiang, J. Liang, P. W. Noble, *Physiol. Rev.* **2011**, *91*, 221; b) M. Erickson, R. Stern, *Biochem. Res. Int.* **2012**, *2012*, 893974.
27. T.-H. Tran, R. Rastogi, J. Shelke, M. M. Amiji, *Sci. Rep.* **2015**, *5*, 1.
28. M.-A. Shahbazi, M. Sedighi, T. s. Bauleth-Ramos, K. Kant, A. Correia, N. Poursina, B. Sarmento, J. Hirvonen, H. l. A. Santos, *Acs Omega* **2018**, *3*, 18444.
29. Z. Gu, S. H. Chen, Z. Ding, W. Song, W. Wei, S. Liu, G. Ma, R. Zhou, *Nanoscale* **2019**, *11*, 22293.
30. a) W. M. Payne, D. Svechkarev, A. Kyrychenko, A. M. Mohs, *Carbohydr. Polym.* **2018**, *182*, 132; b) E. Alimohammadi, M. Khedri, A. M. Jahromi, R. Maleki, M. Rezaian, *Int. J. Nanomed.* **2020**, *15*, 6887.
31. C. A. Söldner, A. H. Horn, H. Sticht, *Sci. Rep.* **2018**, *8*, 1.
32. F. Kong, H. Zhang, X. Zhang, D. Liu, D. Chen, W. Zhang, L. Zhang, H. A. Santos, M. Hai, *Adv. Funct. Mater.* **2016**, *26*, 6158.
33. N. Dehneshin, H. Raissi, Z. Hasanzade, F. Farzad, *J. Mol. Model.* **2019**, *25*, 1.
34. a) E. M. Bachelder, T. T. Beaudette, K. E. Broaders, J. Dashe, J. M. Fréchet, *J. Am. Chem. Soc.* **2008**, *130*, 10494; b) Z. Lin, J. Li, H. He, H. Kuang, X. Chen, Z. Xie, X. Jing, Y. Huang, *RSC Adv.* **2015**, *5*, 9546; c) H. Kuang, Y. Wu, Z. Zhang, J. Li, X. Chen, Z. Xie, X. Jing, Y. Huang, *Polym. Chem.* **2015**, *6*, 3625.
35. a) E. R. Gillies, A. P. Goodwin, J. M. Fréchet, *Bioconjugate Chem.* **2004**, *15*, 1254; b) J. L. Cohen, S. Schubert, P. R. Wich, L. Cui, J. A. Cohen, J. L. Mynar, J. M. Fréchet, *Bioconjugate Chem.* **2011**, *22*, 1056.
36. a) S. W. Kim, K. T. Oh, Y. S. Youn, E. S. Lee, *Colloids Surf. B* **2014**, *116*, 359; b) W. Xu, J. Qian, G. Hou, A. Suo, Y. Wang, J. Wang, T. Sun, M. Yang, X. Wan, Y. Yao, *ACS Appl. Mater. Interfaces* **2017**, *9*, 36533; c) R. Hu, H. Zheng, J. Cao, Z. Davoudi, Q. Wang, *J. Biomed. Nanotechnol.* **2017**, *13*, 1058.
37. W. Ma, S. Rajabzadeh, A. R. Shaikh, Y. Kakihana, Y. Sun, H. Matsuyama, *J. Membr. Sci.* **2016**, *514*, 429.
38. a) N. Bertrand, P. Grenier, M. Mahmoudi, E. M. Lima, E. A. Appel, F. Dormont, J.-M. Lim, R. Karnik, R. Langer, O. C. Farokhzad, *Nat. Commun.* **2017**, *8*, 1; b) S. Tenzer, D. Docter, J. Kuharev, A. Musyanovych, V. Fetz, R. Hecht, F. Schlenk, D. Fischer, K. Kiouptsi, C. Reinhardt, *Nat. Nanotechnol.* **2013**, *8*, 772.
39. a) R. L. Pinals, D. Yang, D. J. Rosenberg, T. Chaudhary, A. R. Crothers, A. T. Iavarone, M. Hammel, M. P. Landry, *Angew. Chem.* **2020**, *132*, 23876; b) H. Lee, *Pharmaceutics* **2021**, *13*, 637.
40. E. Cadenas, L. Packer, *Thiol Redox Transitions in Cell Signaling, Part A: Chemistry and Biochemistry of Low Molecular Weight and Protein Thiols*, Academic Press, **2010**.
41. G. Settanni, J. Zhou, T. Suo, S. Schöttler, K. Landfester, F. Schmid, V. Mailänder, *Nanoscale* **2017**, *9*, 2138.
42. O. Vilanova, J. J. Mittag, P. M. Kelly, S. Milani, K. A. Dawson, J. O. Rädler, G. Franzese, *ACS Nano.* **2016**, *10*, 10842.
43. F. Tavanti, A. Pedone, M. C. Menziani, *J. Phys. Chem. C* **2015**, *119*, 22172.
44. N. A. Azman, T. X. Nguyen, J. C. Y. Kah, *J. Phys. Chem. B* **2021**, *125*, 1181.

How to cite this article: M. Khedri, F. Afsharchi, A. H. Souderjani, S. Rezvantalab, M. Didandeh, R. Maleki, K. Musaie, H. A. Santos, M.-A. Shahbazi, *Nano Select*. **2022**, *3*, 1252.
https://doi.org/10.1002/nano.202200043